Centrioles control the capacity, but not the specificity, of cytotoxic T cell killing

Fella Tamzalit[a], Diana Tran[b], Weiyang Jin[c], Vitaly Boyko[d], Hisham Bazzi[e,1], Ariella Kepecs[a], Lance C. Kam[c], Kathryn V. Anderson[e], and Morgan Huse[a,2]

[a]Immunology Program, Memorial Sloan Kettering Cancer Center, New York, NY 10065; [b]Immunology and Microbial Pathogenesis Program, Weill Cornell Medical College, New York, NY 10065; [c]Department of Biomedical Engineering, Columbia University, New York, NY 10027; [d]Molecular Cytology Core Facility, Memorial Sloan Kettering Cancer Center, New York, NY 10065; and [e]Developmental Biology Program, Memorial Sloan Kettering Cancer Center, New York, NY 10065

Edited by Ira Mellman, Genentech, Inc., South San Francisco, CA, and approved January 16, 2020 (received for review August 1, 2019)

Immunological synapse formation between cytotoxic T lymphocytes (CTLs) and the target cells they aim to destroy is accompanied by reorientation of the CTL centrosome to a position beneath the synaptic membrane. Centrosome polarization is thought to enhance the potency and specificity of killing by driving lytic granule fusion at the synapse and thereby the release of perforin and granzymes toward the target cell. To test this model, we employed a genetic strategy to delete centrioles, the core structural components of the centrosome. Centriole deletion altered microtubule architecture as expected but surprisingly had no effect on lytic granule polarization and directional secretion. Nevertheless, CTLs lacking centrioles did display substantially reduced killing potential, which was associated with defects in both lytic granule biogenesis and synaptic actin remodeling. These results reveal an unexpected role for the intact centrosome in controlling the capacity but not the specificity of cytotoxic killing.

T cell | centriole | centrosome | microtubule | cytotoxicity

CTLs and natural killer (NK) cells play critical roles in antiviral and anticancer responses by selectively destroying infected or transformed target cells. The most prevalent mechanism of target cell killing involves the secretion of a cellular venom containing the hydrophobic protein perforin and several granzyme proteases (1, 2). Perforin forms oligomeric pores on the target cell surface, inducing a membrane damage response that allows granzymes to access the cytoplasm where they cleave specific substrates to induce apoptosis (3). Essentially all cell types are sensitive to this mode of killing. Hence, specialized mechanisms have evolved to ensure that the effects of perforin and granzyme are constrained to the target cell alone.

Cytotoxic lymphocytes store perforin and granzyme in specialized secretory lysosomes called lytic granules (2, 3), whose low pH environment quenches the activity of both proteins. Within minutes of target cell recognition, lytic granules traffic along microtubules to the stereotyped interface between the lymphocyte and the target cell, which is known as the immunological synapse (IS). Here, they fuse with the plasma membrane to release their contents into the intercellular space. Concomitantly, cortical F-actin at the IS undergoes dramatic remodeling, generating a complex landscape of highly dynamic sheets and protrusions (4). Recent studies indicate that these structures boost the lytic activity of perforin by applying mechanical force against the target cell (5, 6).

Effective killing depends on the exclusive release of granule contents at the IS. This concentrates the perforin and granzymes delivered to the target while simultaneously minimizing damage to bystander cells in the surrounding tissue. Directional granule release (also called degranulation) is generally thought to depend on the centrosome, a membraneless organelle that serves as the microtubule-organizing center (MTOC) in most cells (7, 8). Microtubules radiate from the centrosome with their minus ends directed inward and their plus ends outward. Metazoan centrosomes contain, at least, two centrioles, which are cylindrical structures made of parallel microtubule triplets, surrounded by a cloud of proteinaceous pericentriolar material (PCM). The centrioles maintain centrosomal organization, while the PCM, which is highly enriched in γ-tubulin, is responsible for nucleating microtubule growth. A defining feature of IS formation is the movement of the centrosome to a position just beneath the center of the interface. Lytic granules cluster around the centrosome in activated lymphocytes, and, therefore, its reorientation to the IS positions the granules close to the synaptic membrane (2, 9). The temporal coordination among granule clustering, centrosome reorientation, and target cell killing implies that the centrosome delivers the granules to the IS for fusion, thereby maintaining the potency and specificity of the response. Consistent with this model, multiple studies have associated delayed or impaired centrosome reorientation with reduced cytotoxicity (10–13). Furthermore, deletion of Cep83, a centrosomal protein required for centriole docking with the plasma membrane, was found to inhibit CTL degranulation (14). Other studies, however, have suggested that robust CTL and NK cell-mediated killing occurs in the absence of centrosome polarization (15–17). Hence, the precise role of the centrosome during cytotoxic responses remains unsettled.

Significance

CTLs fight intracellular pathogens and cancer by forming a close cell–cell interaction, called the immunological synapse with an infected or transformed target cell and then releasing toxic proteins directionally into the synaptic space. Directional secretion is thought to depend on the polarization of the CTL centrosome to a position just beneath the center of the synapse. We show here that CTLs lacking centrioles, which are the core structural components of centrosomes, unexpectedly retain the capacity for polarized secretion. Nevertheless, they kill target cells poorly because they fail to package toxic proteins effectively and form properly organized synapses. This paper establishes novel links among the centrosome, organelle maturation, and the dynamic architecture of cell–cell interfaces.

Author contributions: F.T., D.T., L.C.K., and M.H. designed research; F.T., D.T., W.J., V.B., A.K., and M.H. performed research; W.J., H.B., L.C.K., and K.V.A. contributed new reagents/analytic tools; F.T., D.T., and M.H. analyzed data; and F.T., K.V.A., and M.H. wrote the paper.

The authors declare no competing interest.

This article is a PNAS Direct Submission.

[1]Present address: Cologne Cluster of Excellence in Cellular Stress Responses in Aging-Associated Diseases (CECAD), University of Cologne, 50931 Cologne, Germany.

[2]To whom correspondence may be addressed. Email: husem@mskcc.org.

This article contains supporting information online at https://www.pnas.org/lookup/suppl/doi:10.1073/pnas.1913220117/-/DCSupplemental.

First published February 10, 2020.

In the present paper, we employed a genetic strategy to delete centrioles from CTLs and thereby investigate the importance of an intact centrosome for CTL function. Centriole deletion markedly reduced cytotoxicity as expected. This defect, however, did not result from impaired directional secretion. Indeed, lytic granule trafficking and release remained polarized toward the IS. Rather, centriole deficient CTLs exhibited dysregulated granule biogenesis, which diminished their steady state perforin and granzyme stores and limited their cytotoxic potential. Centriole loss also impaired synaptic F-actin remodeling, reducing force exertion across the IS. These results demonstrate that centrioles control the capacity but not the specificity of target cell killing and reveal an unexpected link between microtubule and F-actin dynamics during T cell activation.

Results

***Sas4*$^{-/-}$*Trp53*$^{-/-}$ CTLs Lack Centrioles and Exhibit Perturbed Centrosome and Microtubule Architecture.** The centriolar adaptor protein spindle assembly defective-4 (SAS4; also called CENPJ) is required for the formation and maintenance of centrosomes in eukaryotes (18, 19). In the absence of SAS4, most cell types undergo P53 dependent apoptosis downstream of a mitotic centriole checkpoint (20). Cells lacking both SAS4 and P53, however, are healthy in culture and proliferate at only a slightly slower rate than normal. Hence, to generate CTLs lacking centrioles, we crossed mice bearing conditional "floxed" alleles of *Sas4* and *Trp53* (the P53 gene) with transgenic mice expressing the OT1 T cell receptor (TCR), which recognizes the ovalbumin$_{257–264}$ peptide presented by the class I major histocompatibility complex protein H2-K^b (H2-K^b-OVA). Lymphocytes from OT1-*Sas4*$^{fl/fl}$*Trp53*$^{fl/fl}$ animals were activated in vitro with their cognate antigen and then retrovirally transduced 48 h later to express Cre recombinase (Fig. 1*A*). After 5 to 6 d of additional culturing in the presence of IL2 and fluorescence-activated cell sorting (FACS) for transduced cells, differentiated OT1-*Sas4*$^{-/-}$*Trp53*$^{-/-}$ double knockout (DKO) CTLs were obtained in sufficient numbers for imaging experiments and functional studies (*SI Appendix*, Fig. S1*A*).

Immunocytochemical analysis using antibodies against centrin, a centriole marker, revealed that a majority of DKO CTLs lacked detectable centrioles with most of the remaining cells containing only one centrin$^+$ object (Fig. 1*B*). This phenotype was readily apparent by day 6 (4 d after Cre transduction) and became even more pronounced thereafter (*SI Appendix*, Fig. S1*B*). By contrast, most wild-type (OT1-*Sas4*$^{fl/fl}$*Trp53*$^{fl/fl}$) CTLs contained, at least, two detectable centrioles at all time points examined (Fig. 1*B* and *SI Appendix*, Fig. S1*B*). This is typical for normal cells, which contain between two and four centrioles, depending on the stage of the centrosome cycle (7). wild-type CTLs also exhibited focal accumulation of the PCM proteins pericentrin and γ-tubulin, which tightly colocalized with centrin$^+$ objects. Pericentrin and γ-tubulin staining was less organized in DKO CTLs, often appearing as a smattering of puncta rather than two intensely fluorescent foci (Fig. 1*B* and *SI Appendix*, Fig. S1*C*). Nevertheless, both markers remained clustered on one side of the cell, implying some degree of residual PCM organization in the absence of centrioles. Importantly, *Trp53*$^{-/-}$ CTLs with one functional copy of *Sas4* displayed normal centrosomal architecture (*SI Appendix*, Fig. S2*A*), indicating that the DKO phenotype resulted from SAS4 and not P53 deficiency.

Next, we examined microtubule organization by staining OT1 CTLs on stimulatory coverslips coated with H2-K^b-OVA and ICAM1, a ligand for the $\alpha_L\beta_2$ integrin LFA1. OT1 CTLs form IS-like contacts with these surfaces, complete with centrosome reorientation toward the interface. In wild-type cells, the dense cluster of microtubules radiating from the centrosome was easily observed in z-projection (top view) images (Fig. 1*C*). This cluster was less obvious in DKO CTLs; indeed, quantification of microtubule density as a function of radial position within cells revealed a marked reduction of centralized microtubule organization (Fig. 1*C* and *SI Appendix*, Fig. S1*D*). DKO CTLs did retain some degree of this centralized configuration (magenta arrows in Fig. 1*C*), however, possibly reflecting the persistence of polarized PCM in the space formerly occupied by the centrosome. We also found that centriole loss did not affect the focal architecture of the Golgi apparatus (*SI Appendix*, Fig. S1*E*), consistent with previous work indicating that Golgi organization persists after centrosome ablation (21). Given that PCM and the Golgi can both nucleate microtubules, it is possible that they serve as a rudimentary MTOC in the absence of an intact centrosome. Consistent with this idea, both the residual PCM (detected by pericentrin staining) and the Golgi polarized toward the IS in DKO CTLs (Fig. 1*C* and *SI Appendix*, Fig. S1*E*), much like the centrosome in wild-type cells.

To investigate the architectural consequences of *Sas4* deletion at higher resolution, conjugates between OVA-loaded EL4 cells and either wild-type or DKO OT1 CTLs were imaged by transmission electron microscopy (TEM) (Fig. 1*D*). In wild-type CTLs, centriole pairs, which appeared as orthogonally oriented cylinders of microtubules, were routinely found in close apposition with the synaptic membrane (Fig. 1*D*), in agreement with previous studies (14, 22). Microtubules emanated from the pericentriolar material and closely associated Golgi stacks, typical of MTOC organization. By contrast, serial sectioning through the IS region identified CTLs in the DKO population lacking centriole barrels. However, these cells contained electron dense PCM with microtubules emanating from this area (red arrowheads in Fig. 1*D*), consistent with the light microscopy (Fig. 1*C*). Golgi stacks and lytic granules were closely associated, suggesting that this PCM acted as a MTOC. These structures also appeared close to the synaptic membrane. Taken together, the light microscopy and TEM analysis indicate that DKO CTLs lack centrioles and exhibit altered microtubule architecture, but, nevertheless, are able to organize microtubules and polarize a rudimentary MTOC to the IS.

Centriole Deletion Does Not Block TCR Signaling. Having confirmed that DKO CTLs lack centrioles, we investigated their responses to TCR stimulation. CTLs were mixed with beads containing immobilized H2-K^b-OVA and ICAM1. In DKO CTLs, this induced degradation of IκB and rapid phosphorylation of Erk1/2 and AKT, indicative of strong signaling through the MAP kinase, phosphoinositide 3-kinase, and NFκB pathways (*SI Appendix*, Fig. S3*A*). These responses were largely indistinguishable from those of control CTLs, indicating that centriole loss does not grossly impair TCR signaling. We also examined calcium (Ca^{2+}) influx downstream of the TCR by imaging CTLs loaded with the Ca^{2+} sensitive dye Fura2 on glass surfaces bearing H2-K^b-OVA and ICAM1. DKO CTLs responded as well as, if not better than, control cells in these experiments (*SI Appendix*, Fig. S3*B*), further supporting the conclusion centrioles are not required for T cell activation.

Next, we assessed the effects of *Sas4* deletion on the secretion of the inflammatory cytokine IFN-γ (IFNγ), a well-established downstream response to TCR stimulation. Coincubation of OT1 CTLs with antigen-loaded RMA-s target cells induced robust IFNγ production, which could be detected by both intracellular staining and enzyme-linked immunosorbent assay (ELISA). DKO CTLs consistently generated more IFNγ than their wild-type counterparts (*SI Appendix*, Fig. S3*C*). We did not observe this phenotype in OT1-*Sas4*$^{+/-}$*Trp53*$^{-/-}$ CTLs, indicating that it resulted from *Sas4* deletion (*SI Appendix*, Fig. S2*B*). Although we cannot currently explain why DKO CTLs make more IFNγ, it is possible that it is related to their enhanced Ca^{2+} responses (*SI Appendix*, Fig. S3*B*). We also examined TCR-induced cell division by stimulating wild-type and DKO CTLs with OVA-loaded splenocytes. Although both cell types exhibited strong proliferation in these experiments, cell division was somewhat delayed in DKO

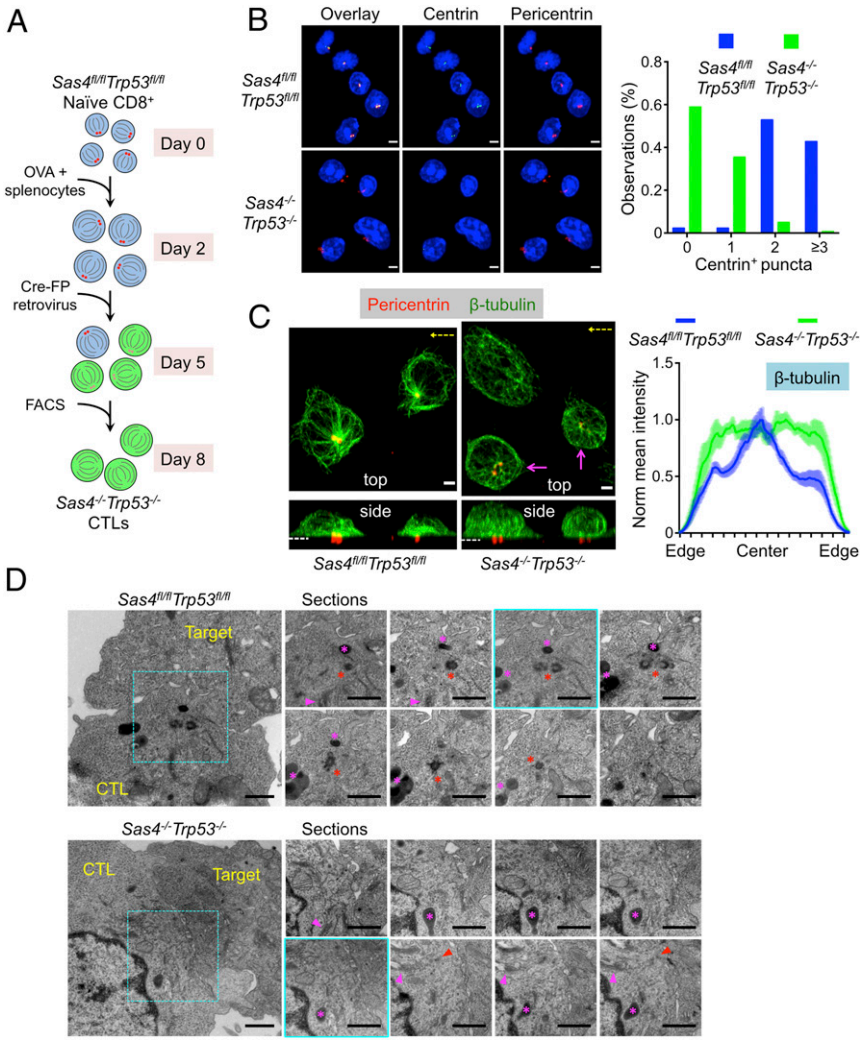

Fig. 1. *Sas4*$^{-/-}$*Trp53*$^{-/-}$ CTLs lack centrioles and display altered microtubule architecture. (*A*) Protocol for generating OT1 *Sas4*$^{-/-}$*Trp53*$^{-/-}$ CTLs. FP indicates GFP, CFP, or RFP. (*B*, *Left*) Representative confocal images of *Sas4*$^{fl/fl}$*Trp53*$^{fl/fl}$ and *Sas4*$^{-/-}$*Trp53*$^{-/-}$ OT1 CTLs stained with antibodies against the indicated centriolar and centrosomal proteins. Nuclear DAPI staining is shown in blue. (Scale bars, 3 μm.) (*B*, *Right*) Quantification of centrin^{+} puncta in *Sas4*$^{fl/fl}$*Trp53*$^{fl/fl}$ (n = 89) and *Sas4*$^{-/-}$*Trp53*$^{-/-}$ (n = 142) OT1 CTLs. (*C*, *Left*) Representative confocal images of *Sas4*$^{fl/fl}$*Trp53*$^{fl/fl}$ and *Sas4*$^{-/-}$*Trp53*$^{-/-}$ OT1 CTLs stained with antibodies against pericentrin and β-tubulin. Top view (z-projection) images are shown above with corresponding side views (x projections) below. The dotted white lines indicate the plane of the IS in the side views. The axis of rotation used to generate the side view is indicated in yellow in the top views. Magenta arrows indicate CTLs with residual centralized microtubule organization. (Scale bars, 2 μm.) (*C*, *Right*) Normalized mean β-tubulin fluorescence intensity in line scans from one cell edge to the opposite edge (see *SI Appendix*, Fig. S1*D* and *Materials and Methods*, $n \geq 12$ for each cell type). Error bars denote SEM. (*D*) TEM analysis of conjugates formed between *Sas4*$^{fl/fl}$*Trp53*$^{fl/fl}$ or *Sas4*$^{-/-}$*Trp53*$^{-/-}$ OT1 CTLs and OVA-loaded EL4 target cells. Wide view panels of representative conjugates are shown on the *Left* with serial sections of the central synaptic domain (indicated by the dashed cyan box in each wide view image) shown on the *Right*. The section corresponding to the wide view image is outlined in cyan. The red asterisks indicate centrioles in the *Sas4*$^{fl/fl}$*Trp53*$^{fl/fl}$ CTL, and the red arrowheads denote residual clusters of electron dense PCM-like material in the *Sas4*$^{-/-}$*Trp53*$^{-/-}$ CTL. The magenta asterisks and arrowheads indicate lytic granules and Golgi stacks, respectively. (Scale bars, 1 μm.)

cells relative to controls, a difference that was most obvious 48 and 72 h after stimulation (*SI Appendix*, Fig. S3*D*). This phenotype was consistent with previous work indicating that centriole loss extends the time spent in mitosis (20).

Finally, we examined cell surface levels of the TCR and LFA1. TCR expression was consistently higher in DKO CTLs than in wild-type controls (*SI Appendix*, Fig. S4*A*), which potentially explains their enhanced Ca^{2+} and cytokine responses. DKO CTLs exhibited normal ligand-induced TCR down-regulation, however, implying that receptor endocytosis is unaffected by centriole loss (*SI Appendix*, Fig. S4*B*). LFA1 expression, for its part, was identical in both groups of CTLs (*SI Appendix*, Fig. S4*A*). Collectively, these data indicate that, despite lacking centrioles, DKO CTLs express key activating receptors and respond robustly to antigenic stimulation.

Centriole Deletion Reduces Cytotoxic Capacity but Not Cytotoxic Specificity. To assess the importance of centrioles for cytotoxicity, OT1 CTLs were mixed with RMA-s cells that had been loaded with increasing amounts of OVA (Fig. 2*A*). DKO CTLs displayed a dramatic cytotoxicity defect at low effector to target (E:T) ratios (1:10, Fig. 2*B*). At higher E:T (1:1), however, this phenotype was much less apparent (Fig. 2*B*) and even absent in certain experiments. Importantly, OT1-*Sas4*$^{+/-}$*Trp53*$^{-/-}$ CTLs killed normally at both E:T ratios (*SI Appendix*, Fig. S2*C*), implying that the DKO defect resulted from SAS4, rather than P53, deficiency. We also measured cytotoxicity at a single cell level by imaging CTLs and target cells that had been loaded into 50 μm × 50 μm polydimethylsiloxane (PDMS) microwells (*SI Appendix*, Fig. S5*A*). This approach prevents the formation of large cell clusters, enabling observation of individual cytotoxic interactions for an extended

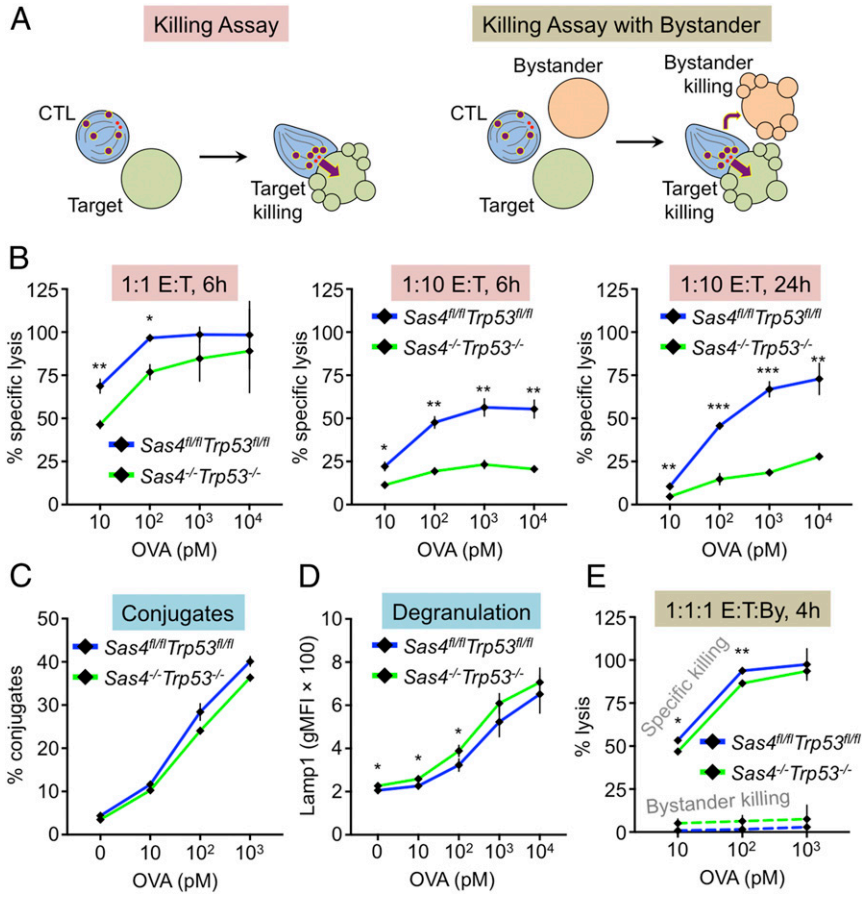

Fig. 2. Centriole loss affects killing capacity but not killing specificity. (*A*) Experimental design for killing assays. (*B–D*) RMA-s target cells were loaded with increasing concentrations of OVA and mixed with *Sas4*$^{fl/fl}$*Trp53*$^{fl/fl}$ or *Sas4*$^{-/-}$*Trp53*$^{-/-}$ OT1 CTLs. Specific lysis of RMA-s cells was assessed at the indicated E:T ratios and times. (*C*) CTL-target cell conjugate formation measured by flow cytometry. (*D*) Degranulation measured by surface exposure of Lamp1. (*E*) RMA-s target cells were loaded with increasing concentrations of OVA and mixed with unpulsed RMA-s cells (bystanders) and either *Sas4*$^{fl/fl}$*Trp53*$^{fl/fl}$ or *Sas4*$^{-/-}$*Trp53*$^{-/-}$ OT1 CTLs at a 1:1:1 ratio. Specific lysis of both targets and bystanders was assessed after 4 h. *P* values (*, **, and ***, indicate $P < 0.05$, $P < 0.01$, and $P < 0.001$, respectively) were calculated by two-tailed Student's *t* test in all panels. Error bars denote SEM.

period of time (10–12 h) (23). Target cell killing was visualized using propidium iodide, a fluorescent DNA intercalating agent, which stains dying cells with compromised plasma membrane integrity. The results of these experiments mirrored those of the bulk assays. In microwells containing only one CTL and one to three target cells, DKO CTLs exhibited a marked killing defect relative to wild-type controls (*SI Appendix*, Fig. S5 *B* and *C*). However, in microwells containing two CTLs and one target, the likelihood of target cell killing was nearly identical. The fact that DKO cytotoxicity was rescued in both bulk and single cell experiments by adding more CTLs suggests that these cells can efficiently kill a small number of targets, but that their potential for extensive serial killing is limited. In other words, our results imply a link between the centriole and the CTL killing capacity.

Effective target cell killing requires that CTLs conjugate tightly with target cells and then degranulate. Conjugate formation, which we measured using a flow cytometry-based approach, was normal in DKO CTLs (Fig. 2*C*). To quantify degranulation, we monitored cell surface exposure of the lysosomal protein Lamp1. TCR stimulation of DKO CTLs induced robust surface expression of Lamp1 that was essentially indistinguishable from the response in wild-type cells (Fig. 2*D*). Hence, the reduced killing capacity of DKO CTLs did not result from impaired conjugate formation or lytic granule release.

Given the purported role of the centrosome in mediating granule polarization to the IS, we hypothesized that centriole loss impairs target cell killing by disrupting the directional secretion of cytotoxic factors. Unpolarized release of perforin and granzyme would be expected to have two functional consequences, 1) reducing the killing of antigen bearing target cells, and 2) increasing the killing of bystander cells. To test the second prediction, we performed cytotoxicity assays in which CTLs were mixed with both OVA-loaded (target) and unloaded (bystander) RMA-s cells at a 1:1:1 ratio (Fig. 2*A*). Surprisingly, DKO CTLs induced little to no bystander cell killing, despite driving robust destruction of bona fide targets (Fig. 2*E*). We observed nearly identical results with wild-type CTLs, implying that both populations kill with equivalent selectivity. Taken together, these results suggest that the CTL centriole controls the capacity but not the specificity of cytotoxic responses.

Microtubules Are Dispensable for Directional Release of Cytotoxic Proteins. The observation that centriole loss did not affect the specificity of killing called into question whether an intact centrosome is actually necessary for polarized lytic granule release at the IS. To investigate this issue, we imaged CTLs that expressed a degranulation reporter comprising a pH sensitive GFP (pHluorin) fused to the C-terminal tail of Lamp1 (24). pHluorin-Lamp1 accumulates in lytic granules where its fluorescence is quenched by the low pH environment. Granule fusion with the plasma membrane, however, neutralizes the pH around the pHluorin, allowing it to fluoresce (Fig. 3*A*). Degranulating CTLs were imaged on

stimulatory glass surfaces coated with H2-K^b-OVA and ICAM1. Degranulation events manifested as abrupt increases in green fluorescence, which often appeared and then disappeared in consecutive time points (Fig. 3*B*). In wild-type cells, degranulations clustered close to the glass surface (within ~2 μm), indicative of synaptic exocytosis (Fig. 3*C*). Remarkably, OT1-DKO CTLs also exhibited highly polarized granule release, implying that centriole loss does not compromise directional secretion.

IS formation is typically associated with the polarization of intracellular granules toward the interface. To quantify this process, we analyzed confocal images of CTLs on both stimulatory (H2-K^b-OVA and ICAM1) and nonstimulatory (ICAM1 alone) surfaces. TCR engagement by H2-K^b-OVA induced a marked shift of lytic granules toward the interface, which we detected by quantifying granzyme B (GzmB) staining intensity as a function of distance from the glass (*SI Appendix*, Fig. S6*A*). Importantly, DKO CTLs polarized their granule pool in a similar manner, despite lacking centrioles. We also observed strong granule accumulation at DKO synapses by TEM (*SI Appendix*, Fig. S6*B*). Hence, centrioles are dispensable for both granule polarization and synaptic secretion.

Both PCM proteins and the Golgi apparatus polarized to the IS in DKO CTLs (Fig. 1*C* and *SI Appendix*, Fig. S1*E*), and it was, therefore, possible that these entities were providing enough microtubule organization to enable granule polarization and directional secretion in the absence of centrioles. To assess the importance of this residual organization, we treated wild-type CTLs with nocodazole, a small molecule that induces microtubule depolymerization. Nocodazole concentrations that eliminated microtubules from the CTL cytoplasm and blocked centrosome reorientation also abrogated the accumulation of lytic granules at the IS (*SI Appendix*, Fig. S6 *C* and *D*), implying an important role for microtubules in delivering granules to the cell surface for secretion. Consistent with this interpretation, overall levels of TCR-induced degranulation were markedly reduced in the presence of nocodazole (Fig. 3*D*). However, the directionality of granule release as revealed by pHluorin-Lamp1 imaging was unaffected. Indeed, although fewer degranulation events were observed in nocodazole-treated CTLs, those that did appear were polarized toward the stimulatory surface to the same extent as in untreated controls (Fig. 3*E*). We also assessed the effect of nocodazole on cytotoxic specificity by performing bystander killing assays. Nocodazole treatment sharply reduced the lysis of OVA-loaded targets, consistent with its capacity to inhibit TCR-induced degranulation (Fig. 3*F*). Bystander killing was unaffected, however, remaining at the same low levels seen in control samples. We conclude that the microtubule cytoskeleton, while it does facilitate cytotoxic secretion, does not, in and of itself, control where lytic granule fusion occurs at the cell surface.

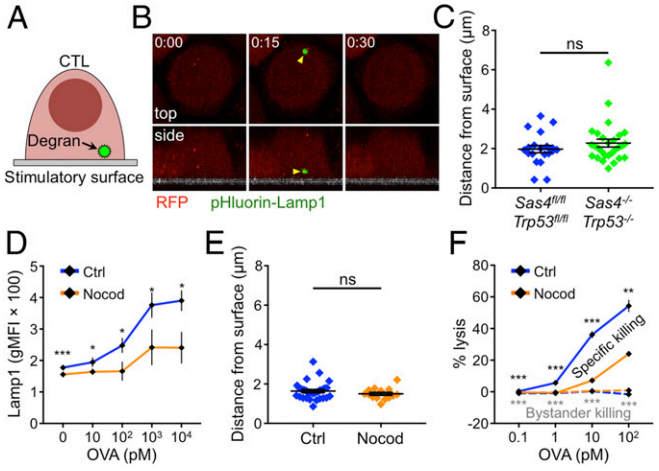

Fig. 3. Microtubules are dispensable for synaptic degranulation. (*A*) pHluorin-Lamp1–based detection of degranulation on stimulatory surfaces. (*B* and *C*) *Sas4*$^{fl/fl}$*Trp53*$^{fl/fl}$ or *Sas4*$^{-/-}$*Trp53*$^{-/-}$ OT1 CTLs expressing RFP and pHluorin-Lamp1 were imaged by confocal microscopy on glass surfaces coated with H2-K^b-OVA and ICAM1. (*B*) A time-lapse montage of a representative degranulation event (yellow arrowhead) with top views shown above and side views shown below. The surface is indicated in gray in the side views. Time in M:SS is shown in the top left corner of each top view image. (*C*) Distance between each degranulation event and the stimulatory surface ($n \geq 20$ for each cell type). (*D*) RMA-s target cells were loaded with increasing concentrations of OVA and mixed with OT1 CTLs in the presence or absence of 30 μM nocodazole. Degranulation was measured by surface exposure of Lamp1. (*E*) OT1 CTLs expressing RFP and pHluorin-Lamp1 were imaged by confocal microscopy on glass surfaces coated with H2-K^b-OVA and ICAM1 in the presence or absence of 30 μM nocodazole. The distance between each degranulation event and the stimulatory surface was measured and graphed ($n \geq 14$ for each cell type). (*F*) RMA-s target cells were loaded with increasing concentrations of OVA and mixed with unpulsed RMA-s cells (bystanders) and OT1 CTLs at a 1:1:1 ratio either in the presence or in the absence of 30 μM nocodazole. Specific lysis of both targets and bystanders was assessed after 4 h. In *C*–*F*, error bars denote SEM. *P* values (*, **, ***, and ns indicate $P < 0.05$, $P < 0.01$, $P < 0.001$, and not significant, respectively) were calculated by two-tailed Student's *t* test in all panels.

Centriole Deletion Impairs Lytic Granule Formation. Because DKO CTLs did not exhibit a defect in directional secretion, we investigated alternative mechanisms that could explain their reduced killing potential. Cytotoxic capacity depends on the amount of perforin and granzyme available for use. Accordingly, we examined the expression of perforin and GzmB and found that DKO CTLs contained markedly reduced levels of both proteins relative to wild-type controls (Fig. 4 *A* and *B*). This phenotype, which was evident by flow cytometry (Fig. 4*A*), immunoblot (Fig. 4*B*), and fluorescence imaging (*SI Appendix*, Fig. S6*A*), manifested in DKO T cells as they differentiated into CTLs and lost their centrioles. At day 5 (3 d after Cre transduction), DKO cells expressed normal amounts of GzmB, but by days 7 and 8 (5 and 6 d after transduction, respectively) GzmB levels were approximately twofold lower than in wild-type cells (Fig. 4*A*). *Sas4*$^{+/-}$*Trp53*$^{-/-}$ CTLs contained normal levels of GzmB (*SI Appendix*, Fig. S2*D*), indicating that the DKO phenotype resulted from SAS4 and not P53 deficiency. DKO CTLs also released less GzmB after TCR stimulation (Fig. 4*C*), indicating that their diminished cytotoxic stores adversely affected their ability to mount secretory responses. DKO CTLs contained equivalent amounts of *Prf1* and *Gzmb* mRNA as controls (Fig. 4*D*), implying that their reduced expression of perforin and GzmB protein resulted from a posttranscriptional defect. We initially considered the possibility that because of centrosomal dysfunction, DKO CTLs might spuriously release lytic granule contents in a TCR independent manner. If this were the case, one would expect to observe higher levels of cytotoxic factors in the culture medium. In fact, we observed more soluble GzmB in wild-type CTL cultures (Fig. 4*E*), arguing against a model of inappropriate granule release.

Reduced perforin and granzyme stores could also be caused by a defect in the maturation of lytic granules. To investigate this possibility, we stained wild-type and DKO CTLs with lysotracker, a dye that labels lysosomal compartments. DKO CTLs exhibited substantially higher levels of lysotracker fluorescence as early as 3 d after Cre transduction (Fig. 5*A*), suggesting that centriole loss actually increases total lysosomal volume. We also assessed lysosome function by incubating CTLs with dye quenched bovine serum albumin (DQ BSA), a fluorogenic protease substrate that is endocytosed readily by cells but only fluoresces upon degradation in lysosomes.

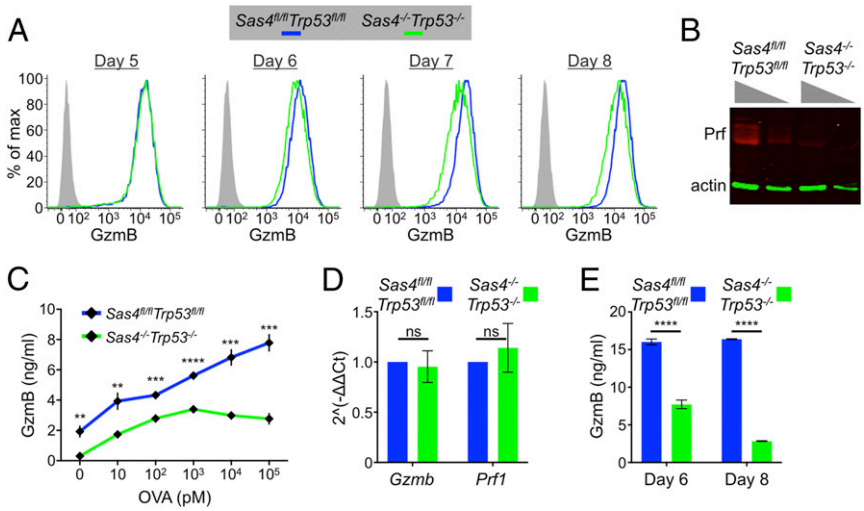

Fig. 4. *Sas4*$^{-/-}$*Trp53*$^{-/-}$ CTLs carry and secrete less cytotoxic cargo. (*A*) *Sas4*$^{fl/fl}$*Trp53*$^{fl/fl}$ naive OT1 T cells were stimulated with OVA-loaded splenocytes and then transduced with Cre-expressing or control retrovirus after 48 h. Subsequently, GzmB expression levels were assessed by flow cytometry in the differentiating CTLs at the indicated time points. (*B*) Perforin expression in day 8 *Sas4*$^{fl/fl}$*Trp53*$^{fl/fl}$ or *Sas4*$^{-/-}$*Trp53*$^{-/-}$ OT1 CTLs was evaluated by immunoblot using actin as a loading control. Two dilutions of each sample were loaded as indicated by the gray triangles. (*C*) RMA-s target cells were loaded with increasing concentrations of OVA and mixed with *Sas4*$^{fl/fl}$*Trp53*$^{fl/fl}$ or *Sas4*$^{-/-}$*Trp53*$^{-/-}$ OT1 CTLs. GzmB levels in the medium after 6 h were assessed by ELISA. (*D*) Quantitative RT-PCR analysis of *Gzmb* and *Prf1* mRNA expression in *Sas4*$^{fl/fl}$*Trp53*$^{fl/fl}$ or *Sas4*$^{-/-}$*Trp53*$^{-/-}$ OT1 CTLs. (*E*) GzmB levels in the culture medium of day 6 and day 8 *Sas4*$^{fl/fl}$*Trp53*$^{fl/fl}$ and *Sas4*$^{-/-}$*Trp53*$^{-/-}$ OT1 CTLs were quantified by ELISA. In *C*–*E*, error bars denote SEM. *P* values (**, ***, ****, and ns indicate $P < 0.05$, $P < 0.001$, $P < 0.0001$, and not significant, respectively) were calculated by two-tailed Student's *t* test in all panels.

DQ-BSA conversion was marginally slower in DKO CTLs than in wild-type controls (*SI Appendix*, Fig. S7*A*), a modest delay that was not caused by differences in endocytosis as both populations robustly internalized tetramethylrhodamine-BSA, a constitutively fluorescent substrate (*SI Appendix*, Fig. S7*A*). Lysosomes also serve as a platform for signaling by the nutrient sensing mTORC1 complex. To assess mTORC1 function, we transferred nutrient-starved CTLs into complete medium and measured the

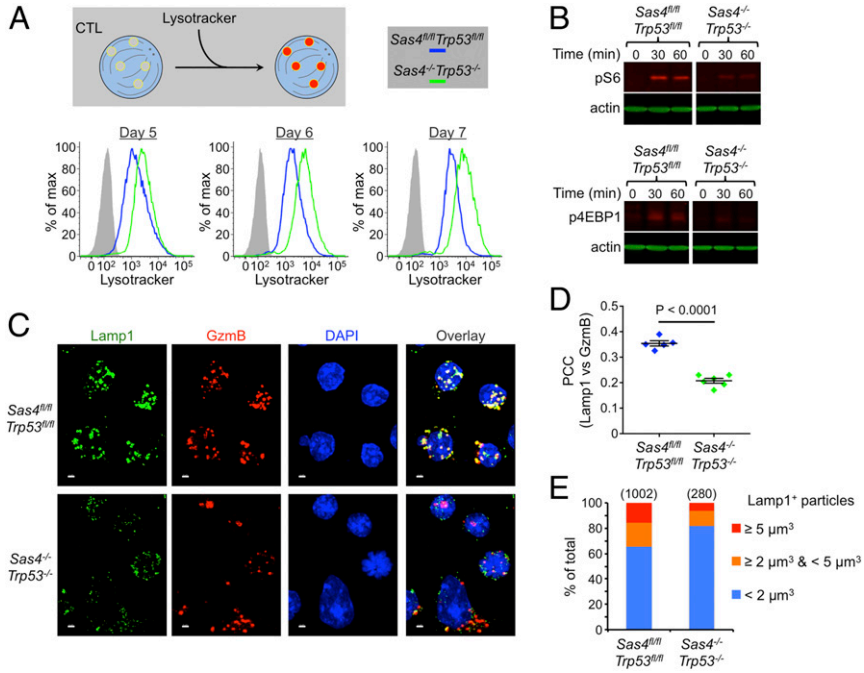

Fig. 5. Centriole loss disrupts lytic granule biogenesis. (*A*) *Sas4*$^{fl/fl}$*Trp53*$^{fl/fl}$ naive OT1 T cells were stimulated with OVA-loaded splenocytes and then transduced with Cre-expressing or control retrovirus after 48 h. Subsequently, lysosomal volume was assessed by lysotracker staining at the indicated time points. (*B*) Serum and nutrient-starved *Sas4*$^{fl/fl}$*Trp53*$^{fl/fl}$ and *Sas4*$^{-/-}$*Trp53*$^{-/-}$ OT1 CTLs were incubated in complete medium for the indicated times after which pS6 kinase and p4EBP1 were assessed by immunoblot using actin as a loading control. (*C*) Representative confocal images of *Sas4*$^{fl/fl}$*Trp53*$^{fl/fl}$ and *Sas4*$^{-/-}$*Trp53*$^{-/-}$ OT1 CTLs stained with antibodies against Lamp1 and GzmB proteins. Nuclear DAPI staining is shown in blue. (Scale bars, 2 μm.) (*D*) PCC between Lamp1 and GzmB fluorescence was determined for each image of *Sas4*$^{fl/fl}$*Trp53*$^{fl/fl}$ and *Sas4*$^{-/-}$*Trp53*$^{-/-}$ OT1 CTLs ($n \geq 5$). Each image contained 10–20 CTLs. *P* value was calculated by two-tailed Student's *t* test. (*E*) Graph showing the distribution of Lamp1^{+} particle size (see *Materials and Methods*) in *Sas4*$^{fl/fl}$*Trp53*$^{fl/fl}$ and *Sas4*$^{-/-}$*Trp53*$^{-/-}$ OT1 CTLs. The number of particles analyzed is indicated in parentheses above each bar.

phosphorylation of S6 kinase and 4EBP1, two canonical mTORC1 substrates. DKO CTLs exhibited markedly reduced mTORC1 activation (Fig. 5*B*), consistent with a defect in lysosomal identity or function. Collectively, these results indicate that centriole deletion alters both the volume and the activity of CTL lysosomes.

To further characterize this phenotype, we imaged CTLs stained for GzmB and the lysosomal protein Lamp1. Both molecules are established markers for lytic granules, and, in wild-type CTLs, they exhibited strong colocalization as expected (Fig. 5*C*). By contrast, many DKO CTLs contained cytoplasmic GzmB puncta with little to no associated Lamp1 staining (Fig. 5*C*). This colocalization defect was confirmed by Pearson's correlation coefficient (PCC) analysis, which revealed significantly reduced overlap between Lamp1 and GzmB (Fig. 5*D*). DKO CTLs also contained a smaller fraction of large Lamp1 puncta, consistent with a defect in the accumulation of Lamp1 in lytic granules (Fig. 5*E*). Centriole loss did not alter the colocalization of Lamp1 with EEA1 and Rab7, which are markers for early and late endosomes, respectively (*SI Appendix*, Fig. S7 *B* and *C*), nor did it affect the size distribution of $EEA1^+$ and $Rab7^+$ compartments (*SI Appendix*, Fig. S7 *B* and *D*). These results implied that the granule organization phenotype seen in DKO CTLs did not result from the dysregulation of endosomal identity but rather from a defect in the maturation of lysosomes into lytic granules. We conclude that centrioles are required for effective granule biogenesis.

Centrioles Regulate Synaptic F-Actin Architecture and Mechanics. The close spatiotemporal coupling between microtubule and F-actin dynamics at the IS raised the possibility that centriole deletion might alter F-actin remodeling. To investigate this hypothesis, we imaged OT1 CTLs by total internal reflection fluorescence microscopy on supported lipid bilayers containing H2-K^b-OVA and ICAM1. wild-type CTLs form radially symmetric synapses with bilayers of this sort that are delimited by a peripheral F-actin rich lamellipodium (Fig. 6 *A* and *B*) (23, 25). LFA1 accumulates at the inner aspect of this F-actin ring, forming a stereotyped "bulls-eye" structure. DKO CTLs exhibited a thicker more irregular band of peripheral F-actin, which was accompanied by constriction of the LFA1 ring (Fig. 6*B*). To quantify this phenotype, we calculated the F-actin "clearance ratio," a parameter that compares the fluorescence intensity at the edges of the IS with that at the center. A clearance ratio less than one is indicative of an annular fluorescence pattern, whereas a clearance ratio of one denotes a uniform distribution. This analysis confirmed that DKO CTLs were significantly impaired in their ability to form synaptic F-actin rings (Fig. 6*C*). We also carried out live imaging experiments using DKO or control CTLs that expressed the F-actin probe Lifeact-GFP. DKO CTLs often formed synapses that lacked an obvious F-actin cleared region at the center, and when these cleared regions did appear, they were more transient than in control CTLs (Fig. 6*D*). Collectively, these data indicated that centriole loss impairs proper F-actin remodeling at the IS.

Synaptic F-actin potentiates cytotoxicity by imparting mechanical force against the target cell (5). Accordingly, we investigated whether the F-actin disruption caused by centriole loss might compromise force exertion at the IS. OT1 CTLs were imaged on arrays of flexible PDMS micropillars that had been coated with H2-K^b-OVA and ICAM1. T cells form IS-like contacts with these arrays, inducing pillar deflections that can be translated into force vectors based on the known dimensions and composition of the pillars (Fig. 6*E*) (26). DKO CTLs exerted significantly less force than their wild-type counterparts (Fig. 6 *F* and *G*), implying that centrosomal integrity is required for F-actin dependent mechanical output at the IS. Taken together with the data in the preceding section, these results indicate that centriole loss undermines killing capacity via two mechanisms by 1) impairing lytic granule biogenesis, and 2) perturbing synaptic force exertion.

Discussion

It is widely thought that the centrosome promotes cytotoxic specificity by guiding lytic granules to the IS for directional secretion (2, 9). To explore this model, we prepared CTLs lacking centrioles, the core structural components of the centrosome. Although this approach altered microtubule architecture, it had no measurable effect on the polarization of lytic granules, the directionality of cytolytic secretion, and the specificity of target cell killing. It did, however, impair lytic granule biogenesis and synaptic F-actin dynamics. These results reveal unexpected roles for centrioles in controlling cytotoxic capacity and IS organization.

Although centriole deletion did perturb the organization of γ-tubulin and pericentrin, these PCM markers remained clustered in most DKO CTLs. TEM analysis of acentriolar cells revealed microtubules emanating from PCM, implying that this residual material retained microtubule-nucleating capacity. Clusters of residual PCM, together with associated microtubules, have also been observed in acentriolar DT40 B cells (27), further supporting the interpretation that they can mediate some degree of microtubule organization. We also note that the Golgi apparatus, which is known to nucleate and organize microtubules on its own (21, 28), retained its focal structure in the absence of centrioles. Importantly, both the Golgi and the residual PCM polarized toward the IS, which is one of the defining properties of the T cell centrosome. Hence, it seems likely that one or both of these structures served as a rudimentary MTOC in DKO CTLs, providing sufficient organization to guide the synaptic accumulation of lytic granules. This architectural redundancy is remarkable, and it highlights the importance of the microtubule cytoskeleton for T cell polarity and function.

The persistence of a rudimentary MTOC potentially explains how CTLs lacking centrioles remain capable of specific killing and directional granule release. It does not explain, however, the surprising functionality of CTLs lacking microtubules altogether. Indeed, while microtubule disassembly with nocodazole reduced the magnitude of degranulation responses, it failed to alter both cytotoxic specificity and directional secretion. These results suggest that the microtubule cytoskeleton, while important for facilitating the efficient delivery of granules to the cell surface, does not control where on the surface the granules fuse. This conclusion is consistent with previous work indicating that target cell killing can occur prior to and in the absence of MTOC polarization (15, 17). If the precise locations of granule docking and fusion are not determined by the microtubule cytoskeleton, we must consider the alternative possibility that these sites are established by mechanisms that operate at the synaptic membrane itself. Degranulation is known to occur in IS domains that have been cleared of F-actin and are, therefore, accessible to fusion competent vesicles (24, 29). The fact that granules do not fuse at actin hypodense regions outside the IS, however, implies that other factors also influence the process. Signaling lipids, such as phosphatidylinositols and diacylglycerol are intriguing candidates in this regard. They control membrane specification, regulated secretion, and polarity in diverse cell types (30, 31), and they play a central role in the patterning of architectural microdomains within the IS (10, 23, 32). Local Ca^{2+} influx, which drives regulated fusion at the neuronal synapse (33), could also be involved. Finally, recent studies have suggested that granule docking and fusion occur close to areas of strong integrin engagement (34), implying that outside-in signal transduction or mechanical tension could define permissive locations for exocytosis.

Although centriole deletion failed to disrupt directional lytic granule secretion in our hands, it did induce a marked and

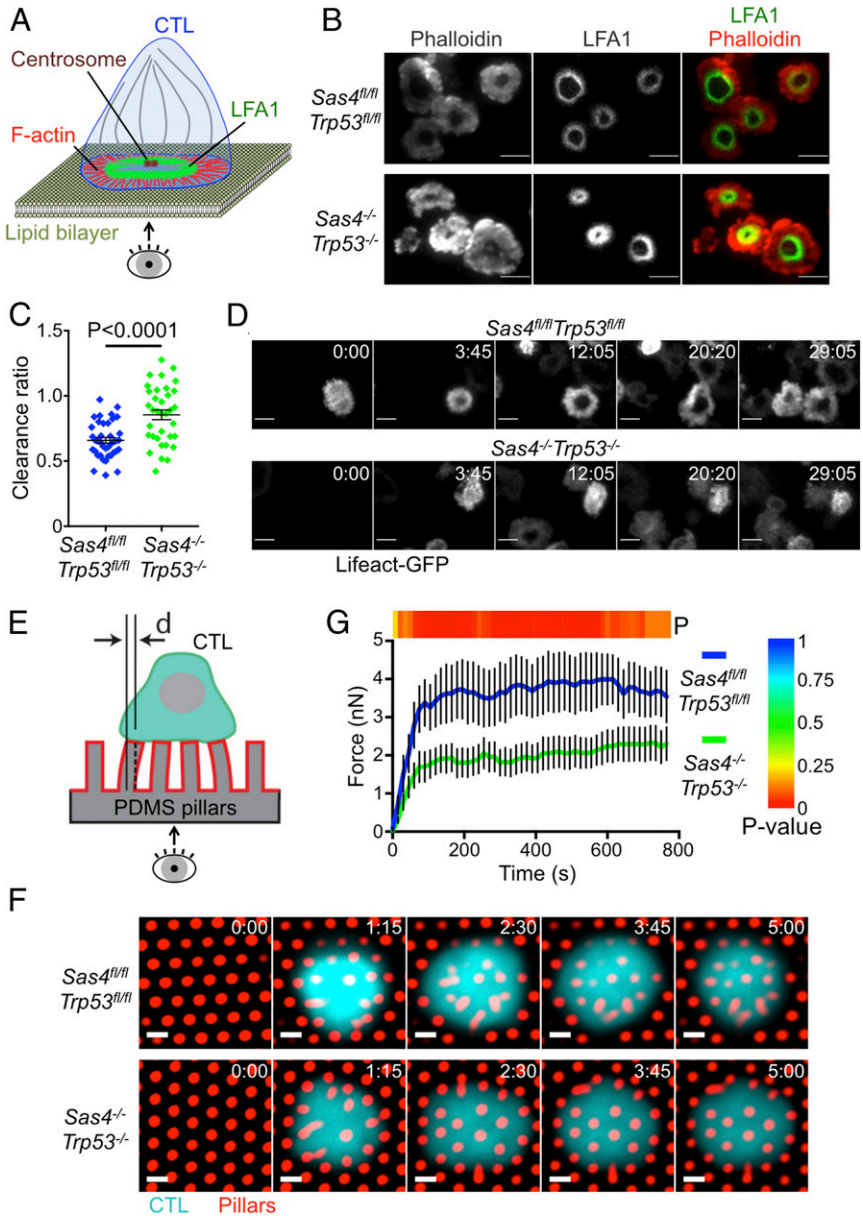

Fig. 6. Centriole loss alters synaptic F-actin configuration and mechanical force exertion. (*A*) IS imaging on supported lipid bilayers. (*B*) *Sas4*$^{fl/fl}$*Trp53*$^{fl/fl}$ and *Sas4*$^{-/-}$*Trp53*$^{-/-}$ OT1 CTLs were added to supported lipid bilayers containing H2-K^{b}-OVA and ICAM1, fixed and stained with phalloidin and antibodies against LFA1. Representative total internal reflection fluorescence (TIRF) images are shown. (Scale bars, 10 μm.) (*C*) F-actin clearance ratio (see *Materials and Methods*) was quantified for each cell ($n \geq 35$ for each cell type). (*D*) Time lapse montages of representative *Sas4*$^{fl/fl}$*Trp53*$^{fl/fl}$ and *Sas4*$^{-/-}$*Trp53*$^{-/-}$ OT1 CTLs forming synapses on supported lipid bilayers containing H2-K^{b}-OVA and ICAM1. F-actin was visualized by TIRF imaging of transduced Lifeact-GFP. Time in MM:SS is indicated in the upper right corner of each image. (Scale bars, 10 μm.) (*E*) Micropillar system to measure synaptic forces. (*F*) *Sas4*$^{fl/fl}$*Trp53*$^{fl/fl}$ and *Sas4*$^{-/-}$*Trp53*$^{-/-}$ OT1 CTLs were labeled with fluorescent anti-CD45 Fab fragments and added to PDMS micropillars coated with H2-K^{b}-OVA and ICAM1. Time-lapse montages of representative cells are shown. Time in M:SS is indicated in the upper right corner of each image. (Scale bars, 2 μm.) (*G*) Total force exertion against pillar arrays graphed versus time ($n \geq 11$ of each cell type). The color bar above the graph indicates the *P* value for each time point. In *C* and *G*, error bars denote SEM. *P* values were calculated by two-tailed Student's *t* test.

unexpected defect in granule biogenesis. DKO CTLs had increased lysosomal volume, but paradoxically exhibited delayed lysosomal degradation, reduced mTORC1 signaling capacity, and lower steady state levels of perforin and GzmB. They also exhibited reduced colocalization between Lamp1 and GzmB, implying a failure to sort cytotoxic proteins into fusion competent granules. Consistent with this interpretation, we found that these cells secreted less GzmB in response to TCR stimulation, despite normal surface exposure of Lamp1. Hence, not only do DKO CTLs store less perforin and granzyme, but also the factors that they do retain are functionally handicapped due to improper compartmentalization. The microtubule cytoskeleton plays a well-established role in the intracellular trafficking of vesicular organelles. In recent years, however, it has become increasingly clear that microtubules are also critical for the maturation and function of these compartments. This is particularly true for lysosomes, whose degradative and signaling capacities depend on their location within the microtubule network (35, 36). Lysosome positioning is known to regulate cell migration and antigen presentation in immune cells (37–39), and it will be interesting

to investigate the extent to which centriole loss affects these processes.

Centrosome dysfunction has been linked to a number of inherited disorders, including polycystic kidney disease and Bardet–Biedl syndrome (40). The pathogenesis of these diseases, which are collectively called ciliopathies, has generally been attributed to defective primary cilia formation and function. Recent studies, however, have raised the possibility that certain symptoms characteristic of ciliopathies might be caused by cilia independent mechanisms, such as disrupted cell polarity and misoriented mitosis (41). It is tempting to speculate that the dysregulation of compartmental identity of the sort observed in this paper might also contribute to disease pathogenesis. In that regard, it is interesting to note that IFT20, an intraflagellar transport protein that is required for primary cilia formation and has been linked to ciliopathies, was recently shown to be required for proper lysosome biogenesis (42).

The defects in synaptic architecture and force exertion observed in DKO CTLs imply an important role for the centrosome in shaping F-actin dynamics at the IS. It is known that the centrosome itself can directly nucleate F-actin (43), which could, in principle, function to organize the lamellipodial and protrusive structures emerging from peripheral IS domains. Alternatively, microtubules emanating from the centrosome could modulate cortical F-actin via proteins that bridge both cytoskeletal networks. In that regard, it is interesting to note that factors operating at the interface between F-actin and microtubules, such as the diaphanous formins and the scaffolding molecule IQGAP, have been implicated in centrosome reorientation and IS assembly (22, 44–46). Close coordination between the centrosome and F-actin could facilitate the efficient organization of synaptic output in space and time. Recent studies suggest that degranulation occurs in synaptic domains that are enriched in LFA1 and that are actively transmitting force against the target cell (6, 34). It will be interesting to investigate the role of the centrosome in ensuring this spatial coupling. Although the centrosome appears to be dispensable for directional secretion, it may yet be critical for linking granule fusion sites to adhesive or mechanically active zones within the IS.

Materials and Methods

The animal protocols used for this study were approved by the Institutional Animal Care and Use Committee of Memorial Sloan Kettering Cancer Center (MSKCC). To prepare OT1-DKO CTLs, naive T cells from OT1 *Sas4*$^{fl/fl}$*Trp53*$^{fl/fl}$ mice were mixed with irradiated C57BL/6 splenocytes pulsed with 100 nM OVA and cultured in Roswell Park Memorial Institute (RPMI) medium containing 10% (vol/vol) fetal calf serum (FCS). Cells were supplemented with 30 IU/mL IL2 after 24 h ,and then, at 48 h, transduced with Cre-expressing or control retrovirus. To prepare the retrovirus, Phoenix E cells were transfected with pMSCV-Cre or empty pMSCV together with packaging plasmids using the calcium phosphate method. Ecotropic viral supernatants were collected after 48 h at 37 °C and added to 1.5×10^6 OT1 blasts. Mixtures were centrifuged at $1,400 \times g$ in the presence of polybrene (4 μg/mL) at 35 °C, and the T cells then split 1:3 in RPMI medium containing 10% (vol/vol) FCS, 30 IU/mL IL2. The following day, 10 μg/mL puromycin was added to the cultures to select for transduced cells. On day 5, transduced CTLs were further enriched by FACS and then cultured at 1.0×10^6 cells/mL in RPMI containing 30 IU/mL IL2. Cultures of CTLs expressing Cre retrovirus were supplemented with the PLK4 inhibitor centrinone B (2 μM, MedChem Express) at day 5 in order to suppress the growth of any residual SAS4$^+$ cells (47). Detailed methods for CTL analysis are described in the *SI Appendix*, which also includes seven supplemental figures.

Data Availability. Data supporting the findings of this paper are available within the article and its *SI Appendix*. Additional data are available from the corresponding author (M.H.) on request.

ACKNOWLEDGMENTS. We thank C. Firl and L. Stafford for technical support; the MSKCC Molecular Cytology Core Facility for assistance with confocal imaging; the MSKCC Monoclonal Antibody Core Facility for fluorescently conjugated F_{ab}; J. Stinchcombe and G. Griffiths (University of Cambridge) for TEM analysis and critical reading of the paper; and J. Xavier (MSKCC), M. Overholtzer (MSKCC), Y. Lee (MSKCC), C. Lee (MSKCC), B. Tsou (MSKCC), M. Marks (University of Pennsylvania), J. K. Burkhardt (University of Pennsylvania), and members of the M.H. Laboratory for advice. This work was supported, in part, by the NIH (grant R01-AI087644 to M.H., grant R01-AI110593 to L.C.K., and grant P30-CA008748 to MSKCC) and the Cancer Research Institute (F.T.).

1. M. L. Dustin, E. O. Long, Cytotoxic immunological synapses. *Immunol. Rev.* **235**, 24–34 (2010).
2. J. C. Stinchcombe, G. M. Griffiths, Secretory mechanisms in cell-mediated cytotoxicity. *Annu. Rev. Cell Dev. Biol.* **23**, 495–517 (2007).
3. J. Thiery, J. Lieberman, Perforin: A key pore-forming protein for immune control of viruses and cancer. *Subcell. Biochem.* **80**, 197–220 (2014).
4. A. T. Ritter *et al.*, Actin depletion initiates events leading to granule secretion at the immunological synapse. *Immunity* **42**, 864–876 (2015).
5. R. Basu *et al.*, Cytotoxic T cells use mechanical force to potentiate target cell killing. *Cell* **165**, 100–110 (2016).
6. Tamzalit F, *et al.*, Interfacial actin protrusions mechanically enhance killing by cytotoxic T cells. *Sci. Immunol.* **4**, eaav5445 (2019).
7. M. Bettencourt-Dias, D. M. Glover, Centrosome biogenesis and function: Centrosomics brings new understanding. *Nat. Rev. Mol. Cell Biol.* **8**, 451–463 (2007).
8. G. A. Pihan, Centrosome dysfunction contributes to chromosome instability, chromoanagenesis, and genome reprograming in cancer. *Front. Oncol.* **3**, 277 (2013).
9. X. Liu, M. Huse, "Immunological synapse formation: Cell polarity during T cell-APC interaction " in *Cell Polarity 1: Biological Role and Basic Mechanisms*, K. Ebnet, Ed. (Springer, Switzerland, 2015), pp. 247–275.
10. E. J. Quann, E. Merino, T. Furuta, M. Huse, Localized diacylglycerol drives the polarization of the microtubule-organizing center in T cells. *Nat. Immunol.* **10**, 627–635 (2009).
11. A. Tsun *et al.*, Centrosome docking at the immunological synapse is controlled by Lck signaling. *J. Cell Biol.* **192**, 663–674 (2011).
12. M. de la Roche *et al.*, Hedgehog signaling controls T cell killing at the immunological synapse. *Science* **342**, 1247–1250 (2013).
13. M. R. Jenkins *et al.*, Distinct structural and catalytic roles for Zap70 in formation of the immunological synapse in CTL. *eLife* **3**, e01310 (2014).
14. J. C. Stinchcombe *et al.*, Mother centriole distal appendages mediate centrosome docking at the immunological synapse and reveal mechanistic parallels with ciliogenesis. *Curr. Biol.* **25**, 3239–3244 (2015).
15. B. Butler, J. A. Cooper, Distinct roles for the actin nucleators Arp2/3 and hDia1 during NK-mediated cytotoxicity. *Curr. Biol.* **19**, 1886–1896 (2009).
16. A. Chauveau, A. Aucher, P. Eissmann, E. Vivier, D. M. Davis, Membrane nanotubes facilitate long-distance interactions between natural killer cells and target cells. *Proc. Natl. Acad. Sci. U.S.A.* **107**, 5545–5550 (2010).
17. F. Bertrand *et al.*, An initial and rapid step of lytic granule secretion precedes microtubule organizing center polarization at the cytotoxic T lymphocyte/target cell synapse. *Proc. Natl. Acad. Sci. U.S.A.* **110**, 6073–6078 (2013).
18. M. Kirkham, T. Müller-Reichert, K. Oegema, S. Grill, A. A. Hyman, SAS-4 is a C. elegans centriolar protein that controls centrosome size. *Cell* **112**, 575–587 (2003).
19. J. Gopalakrishnan *et al.*, Sas-4 provides a scaffold for cytoplasmic complexes and tethers them in a centrosome. *Nat. Commun.* **2**, 359 (2011).
20. H. Bazzi, K. V. Anderson, Acentriolar mitosis activates a p53-dependent apoptosis pathway in the mouse embryo. *Proc. Natl. Acad. Sci. U.S.A.* **111**, E1491–E1500 (2014).
21. A. Efimov *et al.*, Asymmetric CLASP-dependent nucleation of noncentrosomal microtubules at the trans-Golgi network. *Dev. Cell* **12**, 917–930 (2007).
22. J. C. Stinchcombe, E. Majorovits, G. Bossi, S. Fuller, G. M. Griffiths, Centrosome polarization delivers secretory granules to the immunological synapse. *Nature* **443**, 462–465 (2006).
23. A. Le Floc'h *et al.*, Annular PIP3 accumulation controls actin architecture and modulates cytotoxicity at the immunological synapse. *J. Exp. Med.* **210**, 2721–2737 (2013).
24. G. D. Rak, E. M. Mace, P. P. Banerjee, T. Svitkina, J. S. Orange, Natural killer cell lytic granule secretion occurs through a pervasive actin network at the immune synapse. *PLoS Biol.* **9**, e1001151 (2011).
25. T. N. Sims *et al.*, Opposing effects of PKCtheta and WASp on symmetry breaking and relocation of the immunological synapse. *Cell* **129**, 773–785 (2007).
26. K. T. Bashour *et al.*, CD28 and CD3 have complementary roles in T-cell traction forces. *Proc. Natl. Acad. Sci. U.S.A.* **111**, 2241–2246 (2014).
27. J. H. Sir *et al.*, Loss of centrioles causes chromosomal instability in vertebrate somatic cells. *J. Cell Biol.* **203**, 747–756 (2013).
28. P. M. Miller *et al.*, Golgi-derived CLASP-dependent microtubules control Golgi organization and polarized trafficking in motile cells. *Nat. Cell Biol.* **11**, 1069–1080 (2009).
29. A. C. Brown *et al.*, Remodelling of cortical actin where lytic granules dock at natural killer cell immune synapses revealed by super-resolution microscopy. *PLoS Biol.* **9**, e1001152 (2011).
30. T. Balla, Phosphoinositides: Tiny lipids with giant impact on cell regulation. *Physiol. Rev.* **93**, 1019–1137 (2013).
31. A. Shewan, D. J. Eastburn, K. Mostov, Phosphoinositides in cell architecture. *Cold Spring Harb. Perspect. Biol.* **3**, a004796 (2011).

32. C. M. Gawden-Bone *et al*., PIP5 kinases regulate membrane phosphoinositide and actin composition for targeted granule secretion by cytotoxic lymphocytes. *Immunity* **49**, 427–437 e4 (2018).
33. T. C. Südhof, Calcium control of neurotransmitter release. *Cold Spring Harb. Perspect. Biol.* **4**, a011353 (2012).
34. R. Houmadi *et al*., The Wiskott-Aldrich syndrome protein contributes to the assembly of the LFA-1 nanocluster belt at the lytic synapse. *Cell Rep.* **22**, 979–991 (2018).
35. J. Pu, C. M. Guardia, T. Keren-Kaplan, J. S. Bonifacino, Mechanisms and functions of lysosome positioning. *J. Cell Sci.* **129**, 4329–4339 (2016).
36. V. I. Korolchuk *et al*., Lysosomal positioning coordinates cellular nutrient responses. *Nat. Cell Biol.* **13**, 453–460 (2011).
37. M. I. Yuseff *et al*., Polarized secretion of lysosomes at the B cell synapse couples antigen extraction to processing and presentation. *Immunity* **35**, 361–374 (2011).
38. A. Alloatti *et al*., Toll-like receptor 4 engagement on dendritic cells restrains phagosome fusion and promotes cross-presentation of antigens. *Immunity* **43**, 1087–1100 (2015).
39. M. Bretou *et al*., Lysosome signaling controls the migration of dendritic cells. *Sci. Immunol.* **2**, eaak9573 (2017).
40. J. F. Reiter, M. R. Leroux, Genes and molecular pathways underpinning ciliopathies. *Nat. Rev. Mol. Cell Biol.* **18**, 533–547 (2017).
41. A. Vertii, A. Bright, B. Delaval, H. Hehnly, S. Doxsey, New frontiers: Discovering cilia-independent functions of cilia proteins. *EMBO Rep.* **16**, 1275–1287 (2015).
42. F. Finetti *et al*., The intraflagellar transport protein IFT20 controls lysosome biogenesis by regulating the post-Golgi transport of acid hydrolases. *Cell Death Differ.* **27**, 310–328 (2020).
43. F. Farina *et al*., The centrosome is an actin-organizing centre. *Nat. Cell Biol.* **18**, 65–75 (2016).
44. J. A. Gorman *et al*., The cytoskeletal adaptor protein IQGAP1 regulates TCR-mediated signaling and filamentous actin dynamics. *J. Immunol.* **188**, 6135–6144 (2012).
45. T. S. Gomez *et al*., Formins regulate the actin-related protein 2/3 complex-independent polarization of the centrosome to the immunological synapse. *Immunity* **26**, 177–190 (2007).
46. L. Andrés-Delgado *et al*., INF2 promotes the formation of detyrosinated microtubules necessary for centrosome reorientation in T cells. *J. Cell Biol.* **198**, 1025–1037 (2012).
47. Y. L. Wong *et al*., Cell biology. Reversible centriole depletion with an inhibitor of Polo-like kinase 4. *Science* **348**, 1155–1160 (2015).